

See discussions, stats, and author profiles for this publication at: <https://www.researchgate.net/publication/229112442>

# Enhanced Dopant Solubility and Visible-Light Absorption in Cr<sub>x</sub>N Codoped TiO<sub>2</sub> Nanoclusters

ARTICLE *in* THE JOURNAL OF PHYSICAL CHEMISTRY C · JANUARY 2012

Impact Factor: 4.77 · DOI: 10.1021/jp208834n

---

CITATIONS

28

READS

62

7 AUTHORS, INCLUDING:



Mirco Chiodi

Empa - Swiss Federal Laboratories for Materi...

7 PUBLICATIONS 63 CITATIONS

[SEE PROFILE](#)



Emanuele Cavaliere

Catholic University of the Sacred Heart

31 PUBLICATIONS 191 CITATIONS

[SEE PROFILE](#)



H. H. Weitering

University of Tennessee

136 PUBLICATIONS 3,540 CITATIONS

[SEE PROFILE](#)



Luca Gavioli

Catholic University of the Sacred Heart

76 PUBLICATIONS 764 CITATIONS

[SEE PROFILE](#)

# Enhanced Dopant Solubility and Visible-Light Absorption in Cr–N Codoped TiO<sub>2</sub> Nanoclusters

Mirco Chiodi,<sup>†,‡</sup> Christine Parks Cheney,<sup>§</sup> Paolo Vilmercati,<sup>§</sup> Emanuele Cavaliere,<sup>†</sup> Norman Mannella,<sup>§</sup> Hanno H. Weitering,<sup>§,||</sup> and Luca Gavioli<sup>\*,†,‡</sup>

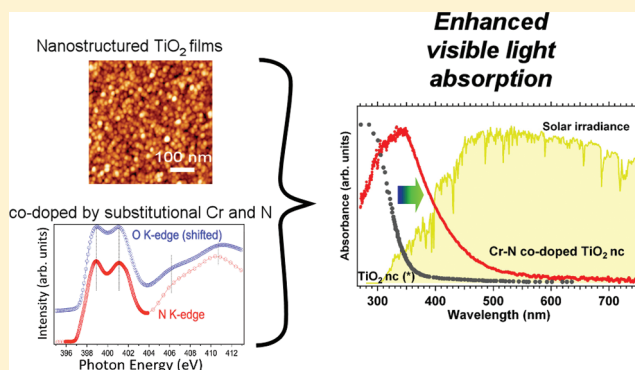
<sup>†</sup>Dipartimento di Matematica e Fisica & Interdisciplinary Laboratories for Advanced Materials Physics (i-LAMP), Università Cattolica del Sacro Cuore di Brescia, Via Musei 41, Brescia 25121, Italy

<sup>‡</sup>Istituto Officina dei Materiali – CNR, Laboratorio TASC, Strada Statale 14, Km.163.5 I-34149 Trieste, Italy

<sup>§</sup>Department of Physics and Astronomy, University of Tennessee, Knoxville, Tennessee 37996-1200, United States

<sup>||</sup>Materials Science and Technology Division, Oak Ridge National Laboratory, Oak Ridge Tennessee 37831, United States

**ABSTRACT:** A major obstacle toward employing TiO<sub>2</sub> as an efficient photoactive material is related to its large optical band gap, strongly limiting visible light absorption. Substitutional doping with both donors and acceptors (codoping) potentially leads to a significant band gap reduction, but the effectiveness of the codoping approach remains limited by the low solubility of dopants inside TiO<sub>2</sub>. Here we show that nanostructured Cr and N codoped TiO<sub>2</sub> thin films can be obtained by supersonic cluster beam deposition (SCBD) with a high concentration of dopants and a strongly reduced band gap. Complementary spectroscopic investigations show that doping effectively occurs in substitutional lattice sites, inducing dopant levels in the gap that are remarkably delocalized. The high surface-to-volume ratio, typical of SCBD nanostructured films, likely facilitates the dopant incorporation. The present results indicate that SCBD films are highly promising photoactive nanophase materials.



## INTRODUCTION

Nanoparticles have emerged as promising alternatives to conventional materials in many branches of science and technology.<sup>1,2</sup> The strong interest toward nanophase materials stems from their unique physical and chemical properties and functionalities that often differ significantly from their bulk counterparts. Many of these unique properties have already been utilized in nanoelectronics,<sup>3</sup> heterogeneous catalysis,<sup>2,4–6</sup> biomedicine,<sup>7</sup> and photovoltaics.<sup>8,9</sup> In particular, TiO<sub>2</sub>-based nanoparticles are being vigorously pursued because of their potential for efficient solar energy harvesting in corrosive environments.<sup>1,10–13</sup> The efficiency of these novel solar energy materials depends on crucial factors such as their ability to absorb visible light<sup>14–16</sup> and their surface-to-volume ratio (SVR).<sup>1</sup> The major drawback in the use of TiO<sub>2</sub> as a photovoltaic or photocatalytic material is its large band gap of  $\sim 3$  eV, which severely limits its ability to absorb visible light.<sup>16</sup>

To enhance visible light absorption in TiO<sub>2</sub>, researchers often resort to chemical doping schemes,<sup>17–19</sup> mostly on a trial-and-error basis. As recently pointed out by Zhu et al., the failure of these attempts is related to the extremely poor solubility of most dopants in TiO<sub>2</sub>.<sup>20</sup> As a consequence, substitutional dopants often form a very small percentage of the overall dopant content, and dopant atoms are mainly located at undesirable interstitial sites or may even form nanophase precipitates, thus compromising the effectiveness of any such attempt.<sup>20</sup> A second crucial

aspect is the nature of the impurity bands generated by doping. On the one hand, localized states would enhance photon absorption, but on the other hand, they would be of no help in providing mobile charge carriers because they also lead to fast recombination processes. Therefore, delocalization of the impurity states is absolutely essential for efficient light-to-current conversion. A recent theoretical work proposed that codoping with donor and acceptor elements would increase the dopants' solubility and reduce the band gap,<sup>20</sup> but this prediction needs to be followed up by a detailed experimental investigation.

In the present work, we obtain TiO<sub>2</sub> nanostructured films at room temperature (RT) via supersonic cluster beam deposition (SCBD), codoped with high concentrations of Cr and N impurities. The TiO<sub>2</sub> cluster films exhibit an optical absorption edge extending well into the visible light region that can be attributed to the high concentration of dopants. A thorough spectroscopic characterization, by means of soft X-ray photoemission spectroscopy (XPS), shows that Cr and N atoms are injected into substitutional sites with concentrations that are remarkably higher than previously achieved using different growth techniques. New electronic states appear inside the TiO<sub>2</sub> band gap, and these states are found to be Cr- and

Received: September 13, 2011

Revised: November 15, 2011

Published: December 01, 2011

N-related. Moreover, we find strong indications that the N-related unoccupied states in the conduction band are significantly delocalized. The films furthermore exhibit a dramatically enhanced visible-light response compared with undoped  $\text{TiO}_2$ , which is attributed to the high concentration of substitutional dopants. To our knowledge, this is the first successful attempt using SCBD to inject both n-type and p-type dopants simultaneously into titania nanoclusters and to obtain high concentrations of substitutional dopants.

## ■ EXPERIMENTAL SECTION

Nanostructured titanium oxide films (the thickness can be tuned in the 10 nm to 1  $\mu\text{m}$  range according to the experimental needs) were deposited at RT under high vacuum (base pressure  $5 \times 10^{-8}$  mbar) conditions by SCBD using a pulsed microplasma cluster source.<sup>21–23</sup> The source produces a beam of nanoclusters (diameters in the range of 2 to 10 nm) in a predominant rutile phase,<sup>22,23</sup> whereas larger clusters deposited on a substrate form films with the anatase structure, thus allowing the growth of a highly porous thin film with a high SVR.<sup>22,23</sup> Cr–N doped samples were obtained from a Ti–Cr alloy (nominal concentration 95–5%) rod using He as a carrier gas. The N is present inside the ablation and cluster condensation chamber and therefore is prone to the discharge (synchronized with the He injection) generating the plasma, thus favoring incorporation inside the nanoclusters. The nominal film thickness and deposition rate were measured during deposition by a quartz microbalance, whereas the actual thickness was obtained ex situ by atomic force microscopy (AFM) (Solver-pro NT-MDT), which was also used to characterize the film morphology. The data were acquired under nitrogen flow in tapping mode with a nominal tip radius below 10 nm.

The films deposited onto oxidized Si(100) substrates were characterized at RT (after growth and/or thermal treatments) by X-ray absorption spectroscopy (XAS), X-ray photoemission spectroscopy (XPS), resonant photoemission spectroscopy (RESPES), and AFM measurements. For optical absorption measurements, we used quartz substrates. Before performing the spectroscopic measurements, the samples were degassed at 150 °C for several minutes in ultrahigh vacuum to decrease strongly the presence of spurious nitrogen and surface hydroxyls. Optical absorption was performed with a homemade apparatus consisting of a high intensity UV-optimized Xenon lamp, collimated on the sample with a UV–vis optical fiber, and an Ocean Optics USB2000 sensor. A reference spectra for clean quartz and the SCBD sample deposited on the quartz substrate was acquired. XAS and RESPES experiments were carried out at the APE<sup>24</sup> beamline at Elettra synchrotron radiation Source in Basovizza (Trieste, Italy) in the photon range of 380–700 eV with a total resolution of ~200 meV. The XPS spectra were acquired by using a monochromatized Al K $\alpha$  X-ray source ( $h\nu = 1486.6$  eV).

## ■ RESULTS AND DISCUSSION

The as-deposited Cr–N– $\text{TiO}_2$  film exhibits a homogeneous and porous structure that does not depend on the substrate used due to the soft landing.<sup>21–23,25</sup> The clusters are well-resolved, and no signs of fragmentation are evident from the AFM analysis (Figure 1). This is a common feature in SCBD films, regardless of the type of compound deposited.<sup>25–27</sup> The clusters appear to be almost spherical, with an average lateral size below 10 nm. The average particle size was obtained from scanning tunneling

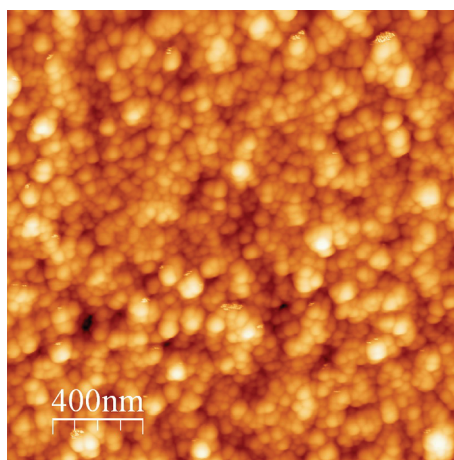


**Figure 1.** AFM image ( $2 \times 2 \mu\text{m}^2$ ) taken in tapping mode on the SCBD Cr–N doped  $\text{TiO}_2$  film deposited on quartz.

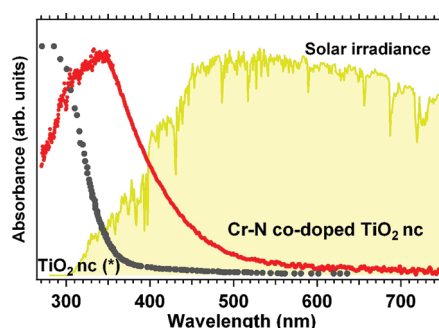


**Figure 2.** Optical absorption spectra taken from the Cr–N codoped nanoclusters (red spectrum) and from an undoped  $\text{TiO}_2$  nanocluster film taken from the literature<sup>25</sup> (gray). Also, the solar spectrum measured at the earth's crust is plotted in the background (orange spectrum). Compared with the undoped  $\text{TiO}_2$  case, the codoped SCBD film's absorbance exhibits a dramatic enhancement in the visible region. The absorption intensity decrease below 290 nm is due to the weak intensity of the spectrometer lamp in this energy region.

microscopy images (not shown), confirming the high SVR of the film.

The optical absorption measurements are shown in Figure 2 (red curve), together with data from undoped  $\text{TiO}_2$  clusters (gray curve) taken from ref 25, obtained with the same SCBD method. The Cr–N codoped SCBD spectrum reveals a significant shift of the main absorption edge toward visible light wavelengths, with a slope change around 480 nm. To estimate the shift, we applied the method of ref 28 using the plot of  $(\alpha h\nu)^n$  versus  $h\nu$  for  $n = 2$  and  $1/2$ , where  $\alpha$  is the measured absorption coefficient and  $h\nu$  is the photon energy, to determine the band gap. Only the  $n = 2$  case produced a meaningful result. For the undoped  $\text{TiO}_2$  clusters (black spectrum), this procedure produced a band gap of  $3.2 \pm 0.05$  eV; the corresponding value for the Cr–N codoped samples is  $2.21 \pm 0.05$  eV. Moreover, the SCBD Cr–N– $\text{TiO}_2$  spectrum is very smooth, not showing any feature that may be related to the possible presence of  $\text{Cr}_2\text{O}_3$  clusters or nanoparticles.<sup>29</sup> This result indicates a significant reduction of the nanocluster-film band gap (~1.0 eV), so that a greater portion of the solar emission spectrum<sup>30</sup> (orange area in Figure 2) can be harvested, as compared with undoped  $\text{TiO}_2$ .

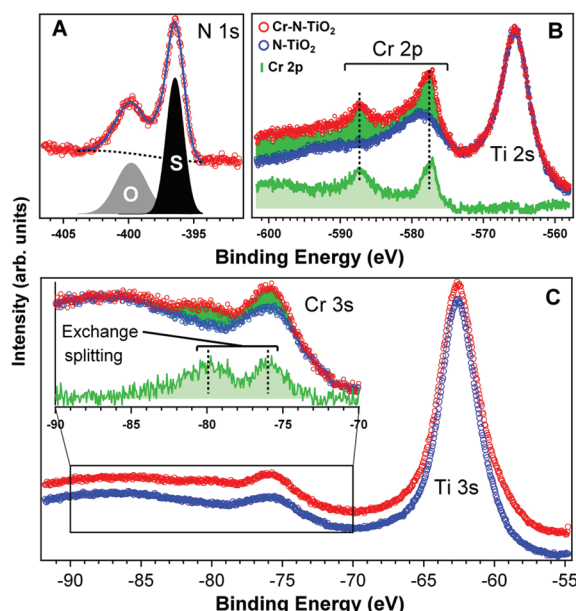


**Figure 3.** (a) N 1s XPS data taken from the Cr–N–TiO<sub>2</sub> nanoclusters (red circles). (b) Ti 2s and Cr 2p core levels spectra taken from the Cr–N–TiO<sub>2</sub> sample (red circles) along with a reference taken from a N-only doped TiO<sub>2</sub> film (blue circles) used to subtract the Ti-related signal. (c) Ti 3s and Cr 3s core level peaks taken from the Cr–N doped (red circles) and N-only doped (blue) samples. Again, the latter was used to isolate the signal originating from the Cr 3s photoelectrons. (See the inset.)

To explain the origin of this band gap reduction, we performed a detailed analysis of the electronic properties of SCBD films. XPS data are presented in Figure 3. The N 1s core level spectrum indicates the presence of N atoms inside the film, producing two different peaks at 396.4 eV ("S" peak in Figure 3A) and 399.8 eV ("O" peak in Figure 3A) binding energy (BE). These two components have been frequently previously reported: the S peak can be attributed to N atoms present in substitutional sites, inside the TiO<sub>2</sub> lattice.<sup>31,32</sup> The O peak attribution is, however, more controversial: features around 400 eV have usually been attributed to molecular nitrogen or oxy-nitride molecules on the surface or inside grain boundaries (see, e.g., ref 32), but atomic interstitial N might also contribute to the peak at 399.8 eV. We emphasize that we do not have evidence of the existence of molecular nitrogen species (observed as a narrow peak at binding energies of ~401.5 eV in TiN and CrN and in N-only doped TiO<sub>2</sub>, respectively<sup>33</sup>) in XAS (see below), so a conclusive assignment cannot be made. However, comparing the intensity of the two peaks, one can clearly conclude that most of the N is present in the highly desirable substitutional sites.

The simultaneous presence of Cr atoms inside our film is confirmed by the Cr 2p core level spectra, plotted in Figure 3B. The spectrum is complicated by the coincidence of the Cr spectra and Ti 2s plasmon loss satellites at ~566 and ~579 eV BE, respectively. To highlight the Cr-related features, we included the spectrum of a TiO<sub>2</sub> nanocluster film doped with only nitrogen. The pure Cr contribution to the spectrum of the Cr–N codoped material was then extracted by subtracting the spectrum of the N-doped TiO<sub>2</sub> material (green spectrum in Figure 3B). The BEs measured for the Cr 2p components (577 and 587 eV) are close to those reported for Cr<sub>2</sub>O<sub>3</sub> (577.1 eV BE)<sup>34</sup> but differ significantly from those reported for Cr–N bonds (574.5 eV BE).<sup>35</sup>

The inspection of the Cr 2p spectrum allows us to conclude that the Cr atoms are incorporated inside the cluster-assembled film, but it does not allow us to identify their atomic sites. To tackle this issue, we determined the Cr valence from the exchange splitting in the Cr 3s core level spectrum. Specifically, the net spin polarization of the valence states leads to an exchange splitting of the Cr 3s spectrum that is proportional to the total spin S of the 3d valence shell.<sup>36</sup> The data taken from the N-only doped and Cr–N-codoped nanoclusters are shown in Figure 3C (blue and red spectra, respectively). As previously described for the Cr 2p spectrum, the contribution due to the nearby Ti 2s peak and its plasmon loss needs to be removed to appreciate fully the contribution originating from the Cr 3s photoelectrons. The results of this procedure are shown in the inset of Figure 3C (green solid line), where two distinct Cr 3s peaks are found at 76 and 80 eV BE (exchange splitting  $\Delta = 4.0$  eV). The separation between the two peaks indicates the presence of Cr<sup>3+</sup> ions, that is, substitutional Cr, as reported for Cr dopants inside TiO<sub>2</sub>.<sup>17,18,37</sup>

The doping concentrations of both Cr and N substitutional impurities with respect to Ti (2p<sub>3/2</sub> BE = 458.9 eV) were obtained from the XPS peak areas weighted by atomic relative sensitivity factors. The spectra were collected with normal emission so as to maximize the probing depth. The stoichiometry of the probed sample volumes was determined from the relative intensities of the core level peaks using standard expressions for the intensities of different core-level peaks<sup>38,39</sup> and theoretical cross sections from Yeh and Lindau.<sup>39</sup> Uncertainties related to the inelastic attenuation lengths of the photoelectrons were alleviated by focusing on core level spectra that are close in kinetic energy, in which case attenuation lengths cancel in the expressions used to determine the stoichiometry. In this way, the substitutional Cr and N concentrations with respect to Ti turned out to be 6 and 11%, respectively. Here the N concentration is remarkably higher than what has been reported for N-doped titania deposited using chemical synthesis methods,<sup>40–43</sup> usually resulting in a maximum substitutional nitrogen content of <2%. Moreover, the current value of 11% is comparable to that obtained for TiO<sub>2</sub> thin films grown by magnetron sputtering.<sup>44</sup> The significant advantage here is that no changes in the nanocluster film morphology have been observed relative to the undoped material, whereas N incorporation significantly affects the morphology of the sputtered thin film<sup>44</sup> and particularly reduces its surface area. The concentration of Cr-only doped TiO<sub>2</sub> systems decreases with increasing post annealing temperatures<sup>17,29,45,46</sup> as a result of surface segregation. Moreover, Cr-doped TiO<sub>2</sub> sol–gel powders exhibit increased defect density and reduced photoactivity due to Cr segregation at the powder surfaces.<sup>47</sup> In our case, XPS (and XAS discussed below) indicates a stable substitutional incorporation of Cr.

This demonstrates that SCBD can significantly enhance the solubility of both dopants into the substitutional sites. This could be related to the formation mechanism inside the SCBD source, in particular, the plasma sputtering of the material, due to a pulsed injection of a carrier gas ionized by an arc discharge, where the incorporation of N during the cluster assembling could take place as well as the high SVR possessed by such cluster-assembled films. The N concentration is roughly independent of the presence of Cr, so there is no clear evidence of Cr–N coupling leading to a higher solid solubility, as recently proposed by Zhu et al.<sup>20</sup>

A deeper description of the Cr and the N behavior in the SCBD films emerges from the analysis of the N K-edge absorption

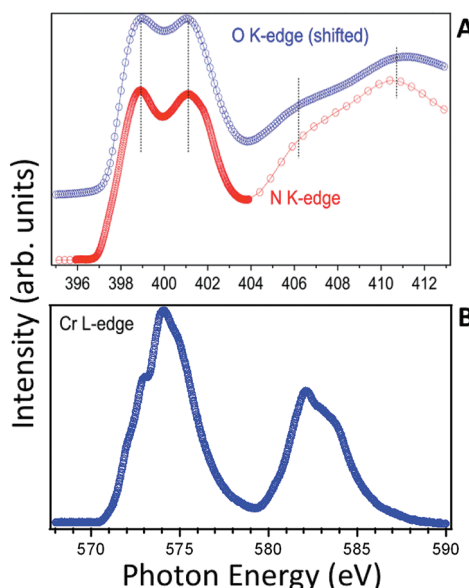


**Figure 4.** XAS data collected from the Cr–N codoped SCBD films. (A) Comparison of the N K-edge absorption spectrum (red circles) with the O K-edge absorption spectrum (blue circles). (B) Cr L-edge absorption data are plotted.

spectrum presented in Figure 4A. The line shape presents two main peaks in the low photon energy region, along with a much broader structure in the 402–413 eV range. The first two peaks are attributed to transitions from the 396 eV N 1s core level to the N 2p–Ti 3d hybridized states.<sup>48</sup> The Ti 3d sub-bands are also split into two separate peaks by the ligand field, giving rise to  $t_{2g}$  and  $e_g$  components.<sup>49</sup> Absorption features arising from the smaller 400 eV N 1s core level component are likely buried under the DOS-like features of the K-edge spectrum. The broad high-energy structure is attributed to transitions to the N 2p – Ti 4sp bands.<sup>50</sup> Interestingly, the spectrum strongly resembles that of titanium nitride (TiN) samples.<sup>48,50</sup> Bearing in mind that XAS measurements are extremely sensitive to the local coordination and the chemical environment surrounding the probed ions,<sup>51</sup> this similarity suggests that the N atoms inside our cluster-assembled film are mainly bonded to Ti atoms, consistent with our previous conclusion from XPS that N atoms are diluted throughout the cluster-assembled film in substitutional sites. We do not have evidence of the existence of molecular nitrogen species in XAS. The latter would have appeared as a very sharp absorption feature, usually at 402 eV,<sup>33</sup> as opposed to the broad DOS-like spectrum observed here. Hence, the 400 eV nitrogen K-edge absorption would be buried underneath the total K-edge spectrum, which has an onset at 397 eV. The same N K-edge XAS spectrum is compared in Figure 4A with the O K-edge spectrum collected from the same SCBD Cr–N–TiO<sub>2</sub> film (shifted to align the first peak of the spectrum to the N K-edge). The N and O XAS data are almost identical, presenting the same ligand-field splitting of 2.3 eV between  $e_g$  and  $t_{2g}$  features. Also, the  $\sigma^*$  part (i.e., beyond 404 eV) appears to be very similar, with two contributions centered around 406.5 and 411.5 eV. Such a common line shape is a strong indication that O and N species are sharing the same coordination by the cations Ti and Cr. Finally, we report the Cr L-edge absorption spectra in Figure 4B. The detailed line shape indicates the presence of Cr<sup>3+</sup>,<sup>52–54</sup> as previously concluded from the Cr 3s core level analysis.

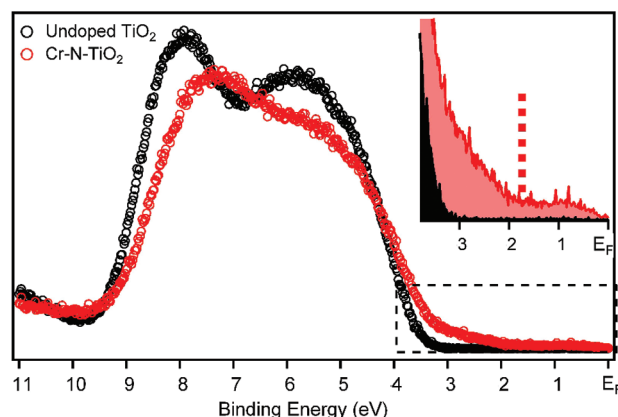


**Figure 5.** Valence band photoemission data taken from the Cr–N codoped TiO<sub>2</sub> nanoclusters (red circles) along with a reference spectrum taken from an undoped TiO<sub>2</sub> film (black). The inset shows a magnification of the VB region, where new occupied states emerge upon doping (with a dotted square line indicating the estimated VB top).

Moreover, comparing our L-edge line shape with that of Cr<sub>2</sub>O<sub>3</sub><sup>54</sup> and CrN<sup>55</sup> one can observe a number of features common to both curves, suggesting that Cr–N and CrO bonds could be present at the same time, whereas to obtain the correct configuration, a detailed simulation would be required.

The introduction of substitutional dopants is expected to give rise to impurity bands that may be responsible for the observed band gap reduction of the TiO<sub>2</sub> host material. The filled-state impurity bands were probed with valence band (VB) photoemission; see Figure 5. The Cr–N-doped TiO<sub>2</sub> cluster-assembled film (red circles) is presented along with a reference spectrum taken from an epitaxial undoped TiO<sub>2</sub> film (black) obtained by pulsed laser ablation. All spectra exhibit the typical O 2s–Ti 3d structure between 4 and 9 eV BE.<sup>31</sup> In the undoped TiO<sub>2</sub>, the main peak is located around 8 eV BE, with a second, less pronounced peak at 5.9 eV. These features appear to be smeared out in the SCBD films: the most intense component is found at 7.4 eV BE, whereas the second feature is visible as a shoulder around 5.5 eV BE. The VB structure's broadening is related to the porous, cluster-assembled structure of the films.<sup>25</sup>

The most important differences can be observed inside the TiO<sub>2</sub> band gap region shown in the inset of Figure 5 from ~3.5 eV BE to  $E_F$ , where additional states appear on the top of the VB upon film doping (red spectrum). The broad peak at 1 eV BE is known to originate from Ti 3d states related to oxygen vacancies.<sup>56</sup> Such states are known to be present in highly defective systems like our SCBD film.<sup>57</sup> They can easily be suppressed by vacuum annealing in an O<sub>2</sub> or N<sub>2</sub> atmosphere, or even by simple air exposure.<sup>31,37</sup> A strong increase in the doping-induced states is observed in the SCBD Cr–N codoped samples as a shoulder appearing around 2.8 eV (red spectrum in the inset of Figure 5). As suggested by the RESPES data discussed below (Figure 6A) and following the detailed analysis for the Cr–TiO<sub>2</sub> system,<sup>37</sup> we attribute this component to Cr 3d states. A rough evaluation of the VB cutoff, obtained by extrapolating the slope of the Cr-induced states, gives a shift of the cutoff of more than 1 eV inside the TiO<sub>2</sub> band gap, apparently as a result of the Cr–N codoping. Hence, if the CB does not exhibit any appreciable variation, then the band gap should be reduced to ~2 eV for the Cr–N codoped SCBD film, in agreement with that estimate from optical absorption data.

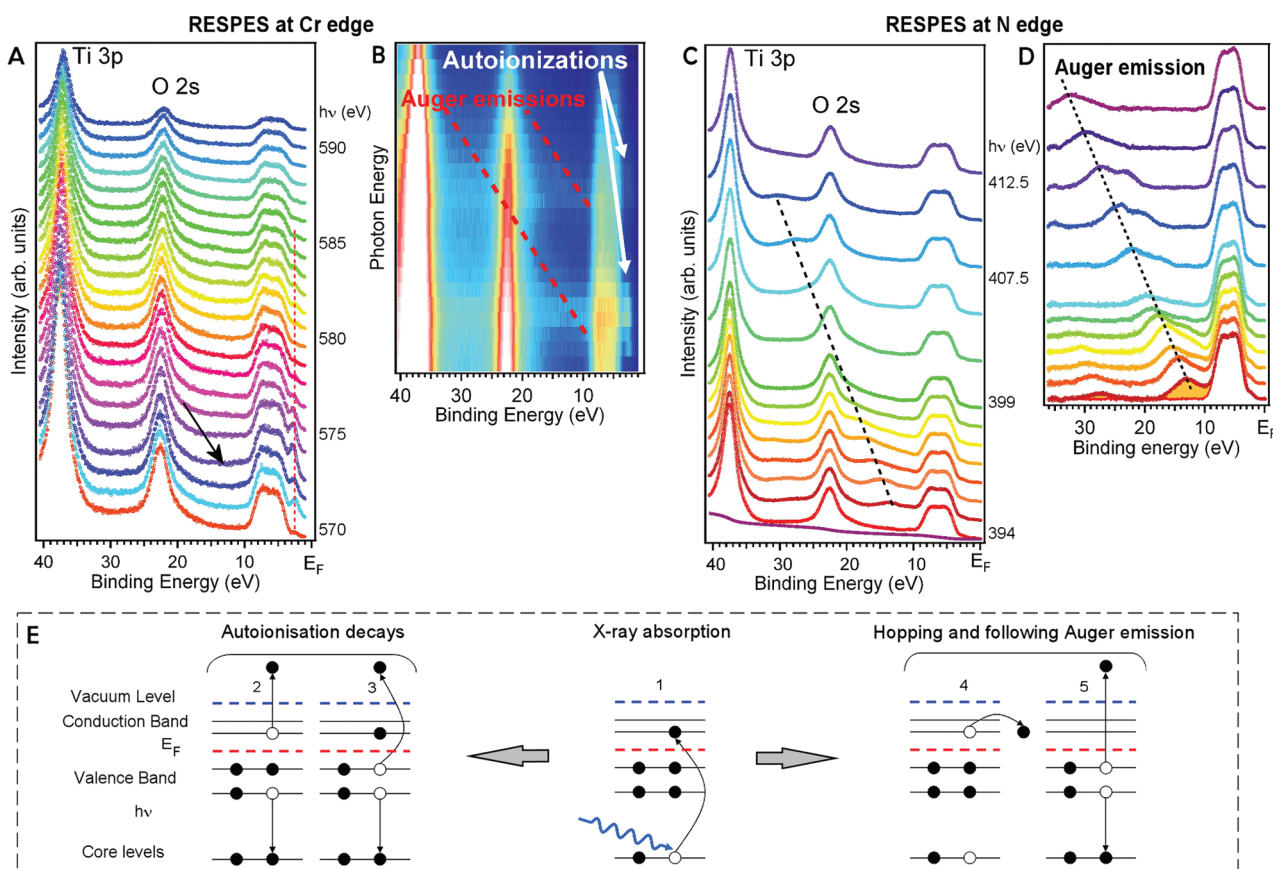


**Figure 6.** (a) Resonant photoemission data collected across the Cr L-edge from the Cr–N codoped TiO<sub>2</sub> SCBD sample: the resonantly enhanced autoionization contribution is evident near 2.5 eV BE (see dotted line); the bottom spectrum is taken at 570 eV photon energy. The arrow marks the onset of a broad and weak Auger feature. Selected photon energies used to acquire the data are indicated on the graph side. (b) Map of the resonant photoemission data presented in panel a, with the autoionization and the weak Auger decays identified. The intensity scale changes from blue (low) to white (high). (c) RESPES data taken across the N K-edge; the dotted line is a guide to the eye to follow the Auger dispersion. Notably, no autoionization contribution is found at the top of the VB. Selected photon energies used to acquire the data are indicated on the graph side. (d) Same data after a Shirley background subtraction and the removal of the Ti 3p and the Os contributions, presented as a function of the binding energy. (e) Resonant photoemission sketch. The absorption of a photon with energy at the edge of an ionization threshold promotes an electron from a core level to the conduction band (1). Such an excited state can decay within a core hole lifetime via autoionization in which the excited electron acts as a participant (2) or a spectator (3). The final states after autoionization decays are the same as those from direct valence band photoemission, and hence these processes interfere quantum mechanically, giving rise to the resonance observed in panel a. If the excited electron delocalizes by hopping faster than a core hole lifetime (4), then the atom will decay by Auger emission (5). In normal Auger decays, the core electron is promoted to the vacuum. In this case, the energy of the incoming radiation is not enough for such a transition to occur. Therefore, this decay can be observed only if an ultrafast delocalization occurs.

To assess any possible benefit for photovoltaic or photocatalytic applications, it is essential to understand the modifications induced by the dopants in the electronic structure of the VB as well as the carrier mobility in the conduction band. This involves precise identification of the impurity states in the VB (Cr- and N-related, in our case) and determining the degree of localization of the Cr- and N-derived empty states. Both of these aspects were evaluated by collecting resonant photoemission data across the Cr L (Figure 6A,B) and the N K (Figure 6C,D) ionization edges. The Cr-edge resonant behavior is presented in Figure 6A, where each spectrum is taken at photon energies indicated in the Figure and in a map of the resonant data (Figure 6B). The VB spectra are very similar to those presented in Figure 5, with a broad O 2p – Ti 3d structure between 4 and 9 eV BE. At higher binding energies, the photoemission spectra show the presence of O 2s (23 eV BE) and Ti 3p (38 eV BE) states.<sup>58</sup> All of these features present a similar intensity decrease as the incident photon energy is increased due to the variation of the photoionization cross

sections for the Ti 3p, O 2s, and VB emissions in the 570–600 eV range.<sup>59</sup>

A strong modulation occurs at the top of the VB, with a peak clearly appearing at ~2.8 eV BE, as the incident photon reaches the Cr resonance value. This resonant behavior unambiguously shows that the states located at the top of the VB are Cr-related. Moreover, as discussed in the literature,<sup>60,61</sup> it is known that core-level resonant photoemission can be exploited to reveal charge-transfer dynamics of a specific system in the low-femtosecond regime. In particular, the evaluation of both the *so-called* autoionization decays and the Auger decay<sup>60,61</sup> can provide insight into the coupling of the specific orbitals under investigation (Cr LUMOs, in our case) with the surrounding environment (Ti-, O-, and N-related orbitals). In addition to the resonant enhancement of the VB spectral feature located at 2.8 eV below the Fermi level, as the photon energy exceeds 573 eV, a weak broad contribution located at ~11 eV appears (Figure 6B, dashed red line). Such a feature does not follow the photon

energy dispersion but is constant in kinetic energy, showing the typical trend of Auger emissions. We stress that emission at this photon energy is forbidden because the excited Cr 2p electron is not promoted to the vacuum level but into an empty state below the vacuum level. (See the sketch in Figure 6E.)<sup>60,61</sup> On the contrary it is a signature of the delocalization of such an empty state. In fact, when an empty state is populated with a core electron, the probability that the electron hops to a neighboring atomic site within a core hole lifetime is determined by the degree of spatial overlap between the selected empty state and the empty states located on the surrounding atoms. If the lifetime of the excited state is long enough, then the core hole will decay through autoionization channels, giving rise to the sharp peak around 2.8 eV constant in BE, whereas if the lifetime of this excited state is shorter than the core-hole lifetime, then the excited electron must have hopped onto a neighboring atomic site, and the core hole will decay through an Auger emission, which is constant in kinetic energy. In this case, the appearance of the clear Cr-related LUMO signature across the Cr resonance together with the Auger decay reveals a competition between the two processes. This in turn suggests that Cr-derived empty states possess a mostly localized character.

The resonant photoemission spectra collected at the N K edge (Figure 6C,D) can be discussed following the same arguments. In this case, as the photon energy matches the ionization threshold, no enhancement of the VB spectral features is observed, focusing in particular on the states at the top of the VB which are N derived p bands (Figure 6C). On the contrary, a clearly visible broad emission is observed at BE = 12 eV for  $h\nu = 394$  eV. To highlight the resonant contribution to the signal, a Shirley background was removed (Figure 6D). Furthermore, the spectrum collected at  $h\nu = 392.5$  eV, that is, below resonance, has been subtracted, and the results are plotted in Figure 6D. Here we have an extreme case in which no autoionization decay is observed, but only Auger emission is detected. This clearly indicates that the hopping (or delocalization) process of the excited charge (schematized in Figure 6E) is dominant with respect to other de-excitation processes. As an upper estimate of the hopping time scale, we consider the lifetime of the core hole that is  $\sim 6$  fs.<sup>62</sup> Such fast hopping would be extremely useful for photoconductivity because it would ultimately facilitate charge collection at the electrodes. Moreover, the high SVR, the strong optical absorption, and the porous nature of the SCBD films make them very promising for photocatalytic applications, where the photogenerated charge can be employed locally to activate chemical reactions. Finally, it also worth noting that nanostructured SCBD films are grown with a method that is environmental friendly because it does not use chemical solvents, and that the films can be easily grown on any substrate maintaining their shape and properties.

## CONCLUSIONS

We have shown that SCBD produces cluster-assembled films of codoped Cr–N TiO<sub>2</sub> with a dramatically enhanced absorbance in the visible region and extending to the near-infrared. The Cr and N dopants are located at the substitutional sites. The increased dopant solubility as compared with other synthesis methods is likely favored by the high SVR of the nanoclusters. The spectroscopic data clearly indicates that the overall effect of the substitutional codoping of both N and Cr species results in the appearance of new electronic states at the top of the VB.

Moreover, we also demonstrated that the N-related orbitals are significantly delocalized.

## AUTHOR INFORMATION

### Corresponding Author

\*E-mail: luca.gavioli@unicatt.it.

## ACKNOWLEDGMENT

We thank Emilia Annese and Ivana Vobornik for their technical support with the synchrotron measurements at Elettra and Gyula Eres for providing TiO<sub>2</sub> samples. This research was partially supported by the U.S. Department of Energy, Basic Energy Sciences, Materials Sciences and Engineering Division (H.H.W.). The work at Elettra was supported by NSF grant DMR-0804902 (N.M.).

## REFERENCES

- (1) Liu, C.; Burghaus, U.; Besenbacher, F.; Wang, Z. L. Preparation and characterization of nanomaterials for sustainable energy production. *ACS Nano* **2010**, *4*, 5517–5526.
- (2) *Handbook of Nanoscience, Engineering and Technology*, 2nd ed.; Goddard, W. A., III, Brenner, D. W., Lyshevski, S. E., Iafrate, G. J., Eds.; CRC Press: Boca Raton, FL, 2007.
- (3) Hiramoto, T.; Saitoh, M.; Tsutsui, G. Emerging nanoscale silicon devices taking advantage of nanostructure physics. *IBM J. Res. Dev.* **2006**, *50*, 411–418.
- (4) Artiglia, L.; Cavaliere, E.; Rizzi, G. A.; Gavioli, L.; Granozzi, G. Probing transformations of relevance in catalysis on a single oxide layer: Fe on TiO<sub>x</sub>/Pt(111). *J. Phys. Chem. Lett.* **2010**, *1*, 1660–1665.
- (5) Huber, G. W.; Chheda, J. N.; Barrett, C. J.; Dumesic, J. A. Production of liquid alkanes by aqueous-phase processing of biomass-derived carbohydrates. *Science* **2005**, *308*, 1446–1450.
- (6) Polshettiwar, V.; Varma, R. S. Green chemistry by nano-catalysis. *Green Chem.* **2010**, *12*, 743–754.
- (7) Boisselier, E.; Astruc, D. Gold nanoparticles in nanomedicine: preparations, imaging, diagnostics, therapies and toxicity. *Chem. Soc. Rev.* **2009**, *38*, 1759–1782.
- (8) Steele, B. C. H.; Heinzel, A. Material for fuel cell technologies. *Nature* **2001**, *414*, 345–352.
- (9) Zhao, J.; Sallard, S.; Smarsly, B. M.; Gross, S.; Bertino, M.; Boissiere, C.; Chen, H.; Shi, J. Photocatalytic performances of mesoporous TiO<sub>2</sub> films doped with gold clusters. *J. Mater. Chem.* **2010**, *20*, 2831–2839.
- (10) Roy, P.; Kim, D.; Lee, K.; Spiecker, E.; Schmuki, P. TiO<sub>2</sub> Nanotubes and their Application in Dye-Sensitized Solar Cells. *Nanoscale* **2010**, *2*, 45–59.
- (11) Weintraub, B.; Wei, Y. G.; Wang, Z. L. Optical fiber/nanowire hybrid structures for efficient three-dimensional dye-sensitized solar cells. *Angew. Chem., Int. Ed.* **2009**, *48*, 8981–8985.
- (12) Carp, O.; Huisman, C. L.; Reller, A. Photoinduced reactivity of titanium oxide. *Prog. Solid State Chem.* **2004**, *32*, 33–177.
- (13) Chen, X. Titanium dioxide nanomaterials and their energy applications. *Chin. J. Catal.* **2009**, *30*, 839–851.
- (14) Schatz, A.; Reiser, O.; Stark, W. J. Nanoparticles as semi-heterogeneous catalyst supports. *Chem.—Eur. J.* **2010**, *16*, 8950–8967.
- (15) Thomas, J. M.; Thomas, W. J. *Principles and Practice of Heterogeneous Catalysis*; Wiley-VCH: Weinheim, Germany, 1996.
- (16) Ruan, C. M.; Paulose, M.; Varghese, O. K.; Mor, G. K.; Grimes, C. A. Fabrication of highly ordered TiO<sub>2</sub> nanotube arrays using an organic electrolyte. *J. Phys. Chem. B* **2005**, *109*, 15754–15759.
- (17) Gracia, F.; Holgado, J. P.; Caballero, A.; Gonzalez-Elipe, A. R. Structure, optical and photoelectrochemical properties of Mn<sup>+</sup>-TiO<sub>2</sub> model thin film photocatalysts. *J. Phys. Chem. B* **2004**, *108*, 17466–17476.
- (18) Kaspar, T. C.; Heald, S. M.; Wang, C. M.; Bryan, J. D.; Droubay, T.; Shuththanandan, V.; Thevuthasan, S.; McCready, D. E.; Kellock, A. J.;

- Gamelin, D. R.; Chambers, S. A. Magnetism in excellent structural quality  $\text{Cr}_x\text{:Ti}_{1-x}\text{O}_2$  anatase: contrast with high- $T_C$  ferromagnetism in structurally defective  $\text{Cr}_x\text{:Ti}_{1-x}\text{O}_2$ . *Phys. Rev. Lett.* **2005**, *95*, 217203–217206.
- (19) Batzill, M.; Morales, E. H.; Diebold, U. Surface studies of nitrogen implanted  $\text{TiO}_2$ . *Chem. Phys.* **2007**, *339*, 36–43.
- (20) Zhu, W. G.; Qiu, X. F.; Iancu, V.; Chen, X. Q.; Pan, H.; Wang, W.; Dimitrijevic, N. M.; Rajh, T.; Meyer, H. M.; Paranthaman, M. P.; Stocks, G. M.; Weitering, H. H.; Gu, B. H.; Eres, G.; Zhang, Z. Y. Band gap narrowing of titanium oxide semiconductors by noncompensated anion-cation codoping for enhanced visible-light photoactivity. *Phys. Rev. Lett.* **2009**, *103*, 226401–226404.
- (21) Mazza, T.; Barborini, E.; Kholmanov, I. N.; Piseri, P.; Bongiorno, G.; Vinati, S.; Milani, P.; Ducati, C.; Cattaneo, D.; Li Bassi, A.; Bottani, C. E.; Taurino, A. jM; Siciliano, P. Libraries of cluster-assembled titania films for chemical sensing. *Appl. Phys. Lett.* **2005**, *87*, 103108–103110.
- (22) Barborini, E.; Kholmanov, I. N.; Piseri, P.; Ducati, C.; Bottani, C. E.; Milani, P. Engineering the nanocrystalline structure of  $\text{TiO}_2$  films by aerodynamically filtered cluster deposition. *Appl. Phys. Lett.* **2002**, *81*, 3052–3054.
- (23) Barborini, E.; Kholmanov, I. N.; Conti, A. M.; Piseri, P.; Vinati, S.; Milani, P.; Ducati, C. Supersonic cluster beam deposition of nanostructured titania. *Eur. Phys. J. D* **2003**, *24*, 277–282.
- (24) Panaccione, G.; Vobornik, I.; Fujii, J.; Krizmancic, D.; Annese, E.; Giovanelli, L.; Maccherozzi, F.; Salvador, F.; De Luisa, A.; Benedetti, D.; Gruden, A.; Bertoč, P.; Polack, F.; Cocco, D.; Sostero, G.; Diviacco, B.; Hochstrasser, M.; Maier, U.; Pescia, D.; Back, C. H.; Greber, T.; Osterwalder, J.; Galaktionov, M.; Sancrotti, M.; Rossi, G. Advanced photoelectric effect experiment beamline at Elettra: a surface science laboratory coupled with synchrotron radiation. *Rev. Sci. Instrum.* **2009**, *80*, 43105–43116.
- (25) Barborini, E.; Conti, A.; Kholmanov, I.; Piseri, P.; Podestà, A.; Milani, P.; Čepel, C.; Sakho, O.; Macovez, R.; Sancrotti, M. Nanostructured  $\text{TiO}_2$  films with 2 eV Optical Gap. *Adv. Mater.* **2005**, *17*, 1842–1846.
- (26) Chioldi, M.; Cavaliere, E.; Kholmanov, I.; de Simone, M.; Sakho, O.; Čepel, C.; Gavioli, L. Nanostructured  $\text{TiO}_x$  film on Si substrate: room temperature formation of  $\text{TiSi}_x$  nanoclusters. *J. Nanopart. Res.* **2010**, *12*, 2645–2653.
- (27) Cassina, V.; Gerosa, L.; Podestà, A.; Ferrari, G.; Sampietro, M.; Fiorentini, F.; Mazza, T.; Lenardi, C.; Milani, P. Nanoscale electrical properties of cluster-assembled palladium oxide thin films. *Phys. Rev. B* **2009**, *79*, 115422–115429.
- (28) Hagfeldt, A.; Gratzel, M. Light-induced redox reactions in nanocrystalline systems. *Chem. Rev.* **1995**, *95*, 49–68.
- (29) Palmisano, L.; Augugliaro, V.; Sclafani, A.; Schiavello, M. Activity of chromium-ion-doped titania for the dinitrogen photoreduction to ammonia and for the phenol photodegradation. *J. Phys. Chem.* **1988**, *92*, 6710–6713.
- (30) Data taken from: SORCE. [http://lasp.colorado.edu/sorce/data/data\\_product\\_summary.htm](http://lasp.colorado.edu/sorce/data/data_product_summary.htm) (accessed Sept 13, 2011).
- (31) Batzill, M.; Morales, E. H.; Diebold, U. Influence of nitrogen doping on the defect formation and surface properties of  $\text{TiO}_2$  rutile and anatase. *Phys. Rev. Lett.* **2006**, *96*, 26103–26106.
- (32) Asahi, R.; Morikawa, T.; Ohwaki, T.; Aoki, K.; Taga, Y. Visible-light photocatalysis in nitrogen-doped titanium oxides. *Science* **2001**, *293*, 269–271.
- (33) Esaka, F.; Furuya, K.; Shimada, H.; Imamura, M.; Matsubayashi, N.; Sato, H.; Nishijima, A.; Kawana, A.; Ichimura, H.; Kikuchi, T. Comparison of surface oxidation of titanium nitride and chromium nitride films studied by x-ray absorption and photoelectron spectroscopy. *J. Vac. Sci. Technol., A* **1997**, *15*, 2521–2528.
- (34) Mischler, S.; Mathieu, H. J.; Landolt, D. Investigation of a passive film on an iron-chromium alloy by AES and XPS. *Surf. Interface Anal.* **1988**, *11*, 182–188.
- (35) Bertóti, I. Characterization of nitride coatings by XPS. *Surf. Coat. Technol.* **2002**, *151*, 194–203.
- (36) Fadley, C. S.; Shirley, D. A.; Freeman, A. J.; Bagus, P. S.; Mallow, J. V. Multiplet splitting of core-electron binding energies in transition-metal ions. *Phys. Rev. Lett.* **1969**, *23*, 1397–1401.
- (37) Nolan, M.; Mulley, J. S.; Bennett, A. Charge transfer in Cr adsorption and reaction at the rutile  $\text{TiO}(2)(110)$  surface. *Phys. Chem. Chem. Phys.* **2009**, *11*, 2156–2160.
- (38) Fadley, C. S. Basic Concepts of X-Ray Photoelectron Spectroscopy. In *Electron Spectroscopy, Theory, Techniques, and Applications*; Brundle, C. R., Baker, A. D., Eds.; Academic Press: New York, 1978; Vol. II, Chapter 1.
- (39) Yeh, J. J.; Lindau, I. At. Data Nucl. Data Tables **1985**, *32*, 1.
- (40) Zhang, S. B. Microscopic origin of the doping limits in semiconductors and wide-gap materials and recent developments in overcoming these limits: a review. *J. Phys.: Condens. Matter* **2002**, *14*, R881–R903.
- (41) Chen, X.; Mao, S. S. Titanium dioxide nanomaterials: synthesis, properties, modifications, and applications. *Chem. Rev.* **2007**, *107*, 2891–2959.
- (42) Fujishima, A.; Zhang, X.; Tryk, D. A.  $\text{TiO}_2$  photocatalysis and related surface phenomena. *Surf. Sci. Rep.* **2008**, *63*, 515–582.
- (43) Nakano, Y.; Morikawa, T.; Ohwaki, T.; Taga, Y. Origin of visible-light sensitivity in N-doped  $\text{TiO}_2$  films. *Chem. Phys.* **2007**, *339*, 20–26.
- (44) Kitano, M.; Funatsu, K.; Matsuoka, M.; Ueshima, M.; Anpo, M. Preparation of nitrogen-substituted  $\text{TiO}_2$  thin film photocatalysts by the radio frequency magnetron sputtering deposition method and their photocatalytic reactivity under visible light irradiation. *J. Phys. Chem. B* **2006**, *110*, 25266–25272.
- (45) Choi, J.; Park, H.; Hoffmann, M. R. Effects of single metal-ion doping on the visible-light photoreactivity of  $\text{TiO}_2$ . *J. Phys. Chem. C* **2010**, *114*, 783–792.
- (46) Li, S.; Jena, P. Origin of the anatase to rutile conversion of metal-doped  $\text{TiO}_2$ . *Phys. Rev. B* **2009**, *79*, 201204.
- (47) Pan, C.-C.; Wu, J. C. S. Visible-light response Cr-doped  $\text{TiO}_2\text{-XN}$  photocatalysts. *Mater. Chem. Phys.* **2006**, *100*, 102–107.
- (48) Esaka, F.; Furuya, K.; Shimada, H.; Imamura, M.; Matsubayashi, N.; Kikuchi, T.; Ichimura, H.; Kawana, A. Composition dependence of the initial oxidation behaviour of  $\text{Ti}_{1-x}\text{Al}_x\text{N}$  ( $x = 0.20, 0.45, 0.65$ ) films studied by XAS and XPS. *Surf. Interface Anal.* **1999**, *27*, 1098–1106.
- (49) De Groot, F. M. F.; Faber, J.; Michiels, J. J. M.; Czyžyk, M. T.; Abbate, M.; Fuggle, J. C. Oxygen 1s X-ray absorption of tetravalent titanium oxides: a comparison with single-particle calculations. *Phys. Rev. B* **1993**, *48*, 2074–2080.
- (50) Chen, H. Y.; Nambu, A.; Wen, W.; Graciani, J.; Zhong, Z.; Hanson, J. C.; Fujita, E.; Rodriguez, J. A. Reaction of  $\text{NH}_3$  with titania: N-doping of the oxide and TiN formation. *J. Phys. Chem. C* **2007**, *111*, 1366–1372.
- (51) de Groot, F. M. F.; Kotani, A. In *Core Level Spectroscopy of Solids*; CRC Press: Boca Raton, FL, 2008.
- (52) de Groot, F. M. F.; Grioni, M.; Fuggle, J. C.; Ghijssen, J.; Sawatzky, G. A.; Petersen, H. *Phys. Rev. B* **1989**, *40*, 5715–5723.
- (53) Theil, C.; van Elp, J.; FolkMann, F. Ligand field parameters obtained from and chemical shifts observed at the Cr L-2,L-3 edges. *Phys. Rev. B* **1999**, *59*, 7931–7936.
- (54) Song, G. S.; Kobayashi, M.; Hwang, J. I.; Kataoka, T.; Takizawa, M.; Fujimori, A.; Ohkouchi, T.; Takeda, Y.; Okane, T.; Saitoh, Y.; Yamagami, H.; Chang, F.-H.; Lee, L.; Lin, H.-J.; Huang, D. J.; Chen, C. T.; Kimura, S.; Funakoshi, M.; Hasegawa, S.; Asahi, H. Electronic structure of  $\text{Ga}_{1-x}\text{Cr}_x\text{N}$  and Si-doping effects studied by photoemission and X-ray absorption spectroscopy. *Phys. Rev. B* **2008**, *78*, 33304–33307.
- (55) Bhobe, P. A.; Chainani, A.; Taguchi, M.; Takeuchi, T.; Eguchi, R.; Matsunami, M.; Ishizaka, K.; Takata, Y.; Oura, M.; Senba, Y.; Ohashi, H.; Nishino, Y.; Yabashi, M.; Tamasaku, K.; Ishikawa, T.; Takenaka, K.; Takagi, H.; Shin, S. Evidence for a correlated insulator to antiferromagnetic metal transition in CrN. *Phys. Rev. Lett.* **2010**, *104*, 236404–236407.
- (56) Diebold, U. The surface science of titanium dioxide. *Surf. Sci. Rep.* **2003**, *48*, 53–229.
- (57) Caruso, T.; Agostino, R. G.; Bongiorno, G.; Barborini, E.; Piseri, P.; Milani, P.; Lenardi, C.; La Rosa, S.; Bertolo, M. Writing submicrometric metallic patterns by ultraviolet synchrotron irradiation of nanostructured carbon and  $\text{TiO}_2$ -carbon films. *Appl. Phys. Lett.* **2004**, *84*, 3412–3414.

(58) Thomas, A. G.; Flavell, W. R.; Kumarasinghe, A. R.; Mallick, A. K.; Tsoutsou, D.; Smith, G. C.; Stockbauer, R.; Patel, S.; Grätzel, M.; Hengerer, R. Resonant photoemission of anatase  $\text{TiO}_2$  (101) and (001) single crystals. *Phys. Rev. B* **2003**, *67*, 035110–035116.

(59) Yeh, J. J. *Atomic Calculation of Photoionization Cross-Sections and Asymmetry Parameters*; Gordon and Breach Science Publishers: Langhorne, PA, 1993.

(60) Bruhwiler, P. A.; Karis, O.; Mårtensson, N. Charge-transfer dynamics studied using resonant core spectroscopies. *Rev. Mod. Phys.* **2002**, *74*, 703–740.

(61) Vilmercati, P.; Cvetko, D.; Cossaro, A.; Morgante, A. Heterostructured organic interfaces probed by resonant photoemission. *Surf. Sci.* **2009**, *603*, 1542–1556.

(62) Chen, W.; Wang, L.; Qi, D. C.; Chen, S.; Gao, X. Y.; Wee, A. T. S. Probing the ultrafast electron transfer at the CuPc/Au(111) interface. *Appl. Phys. Lett.* **2006**, *88*, 184102–184104.